Percutaneous Intramyocardial Septal Ablation with Nanosecond Pulsed Electric Fields in Canine Model

Zhihong Zhao †, Xiangyang Xia †, Jing Li, Yonggang Chen, Gaodong Qiu, Siying Liang, Xinping Lin, Bin Wu, Xinhua Chen *, Zhaoxia Pu *

Posted Date: 27 November 2025

doi: 10.20944/preprints202511.2176.v1

Keywords: nanosecond pulsed electric field; transthoracic echocardiogram; percutaneous intramyocardial septal ablation; myocardial-specific death; safety and efficacy

Article

Percutaneous Intramyocardial Septal Ablation with Nanosecond Pulsed Electric Fields in Canine Model

Zhihong Zhao [1,†], Xiangyang Xia [2,†], Jing Li [2], Yonggang Chen [3], Gaodong Qiu [3], Siying Liang [2], Xinping Lin [2], Bin Wu [3], Xinhua Chen [3,4,*] and Zhaoxia Pu [2,*]

[1] Department of Cardiology, The Affiliated Hospital of Hangzhou Normal University, Hangzhou 310015 China

[2] Department of Cardiology, State Key Laboratory of Transvascular Implantation Devices, State Key Laboratory of Transvascular Implantation Devices, Hangzhou, China

[3] Key Laboratory of Pulsed Power Translational Medicine of Zhejiang Province, Hangzhou 311121, China

[4] Division of Hepatobiliary and Pancreatic Surgery, Department of Surgery, The First Affiliated Hospital, Zhejiang University School of Medicine, Hangzhou 310009, China

* Correspondence: xinhua_chen@zju.edu.cn (X.C.); zhaoxiapu@zju.edu.cn (Z.P.)

† Zhihong Zhao, Xiangyang Xia are co-first authors.

Abstract

Background: Nanosecond pulsed electric field (nsPEF) is a nonthermal ablation technique that utilizes ultra-rapid electrical pulses to induce selective cell death with minimal inflammatory response. The objective of this study was to evaluate the safety and efficacy of percutaneous intramyocardial septal nsPEF ablation (PIMSNA) for septal reduction therapy (SRT) in a canine model (Labrador dogs). **Methods:** The acute and chronic effects of this novel PIMSNA approach under transthoracic echocardiography (TTE) guidance were comprehensively assessed. The optimal ablation parameters for inducing the targeted myocardial pathological process were selected. The major adverse events monitored included post-ablation endocardial regional edema, arrhythmias (e.g., ventricular tachycardia, ventricular fibrillation, atrioventricular conduction block), pericardial effusion, and cardiac tamponade. The assessment of acute and chronic effects was conducted over a 90-day follow-up period using serial TTE imaging, electrocardiographic parameters, blood biochemistry analyses, and histopathological evaluation. The intervention was performed on Labrador canines. **Results:** The experimental findings demonstrated that an applied voltage of 3,000 volts yielded the most effective ablation outcome. TTE-guided PIMSNA procedures resulted in a 10% impedance decline within the targeted region, indicative of successful ablation. The motion amplitude and systolic wall thickening rate demonstrated a substantial decrease and remained persistently low in the ablated septal region. However, septal thickness exhibited no substantial alterations subsequent to PIMSNA. Histological examination confirmed the presence of cardiomyocyte death, characterized by progressive cytoplasmic hyperchromasia and nuclear pyknosis. A notable observation is the minimal presence of acute-phase inflammatory cell infiltration. There were no instances of sustained ventricular tachycardia, ventricular fibrillation, or atrioventricular conduction block during PIMSNA. **Conclusion:** The novel PIMSNA technique effectively induced myocardial injury and regional hypokinesis without significant acute edema. Histopathological analysis revealed significant programmed cell death of cardiomyocytes accompanied by minimal inflammatory cell infiltration.

Keywords: nanosecond pulsed electric field; transthoracic echocardiogram; percutaneous intramyocardial septal ablation; myocardial-specific death; safety and efficacy

 doi:10.20944/preprints202511.2176.v1

1. Introduction

Hypertrophic obstructive cardiomyopathy (HOCM) is a prevalent genetic heart disease found in populations worldwide [1]. The condition is associated with higher morbidity and mortality rates due to left ventricular outflow tract (LVOT) obstruction [2]. For drug-refractory patients, septal reduction therapy (SRT) of the interventricular septum (IVS) is recommended to improve symptoms and prognosis. Alcohol septal ablation is a treatment option that requires appropriate coronary anatomy. The procedure may be less effective for patients with high resting gradients (≥100 mm Hg) and extreme septal thickness (≥30 mm). It is also associated with a greater risk of conduction block, which may require a permanent pacemaker. Furthermore, 7% to 20% of patients may require repeat intervention due to residual obstruction [3,4]. Acute thickening of the ventricular septum caused by local tissue edema is not uncommon during endocardial septal radiofrequency ablation (RFA) [5]. Similarly, transapical beating-heart septal myectomy carries a potential risk of delayed ventricular septal perforation and intraoperative left ventricular apical tear [6]. Percutaneous intramyocardial septal radiofrequency ablation (PIMSRA) in patients with drug-refractory HOCM may be an effective procedure for relief of left ventricular outflow tract obstruction and symptoms with acceptable complication rates [7].

Pulsed Electric Fields (PEF) have emerged as a promising new energy source for cardiac ablation due to its selectivity for cardiac tissue [8]. Nanosecond pulsed electric field (nsPEF) ablation induces irreversible electroporation (IRE) due to the presence of a highly intense electric field. The field exerts a force on the polar molecules present within cell membranes, leading to irreversible permeabilization [9]. nsPEF can penetrate not only cell membranes but also organelles such as the endoplasmic reticulum, mitochondria, and nucleus. Cell responses to nsPEF include calcium mobilization, cytoskeleton destruction, activation of signaling pathways, and induction of apoptosis [10]. The intra-septal pulsed field ablation(PFA) method, with PFA catheter introduced into the right ventricle and directed toward the target lesion. completing ablation without thermal injury to the adjacent tissue [11]. Similar techniques have been used for nsPEF ablation [12].

Percutaneous intramyocardial septal nanosecond pulsed electric field ablation (PIMSNA) is a promising novel technique for SRT. However, the employment of a preclinical large animal model is imperative to confirm its safety and efficacy. The objective of this study was to ascertain the clinical feasibility of PIMSNA by implementing nsPEF in a canine model. The pathological changes were meticulously monitored over a period of up to 90 days.

2. Materials and Methods

2.1. Animal Procedure

The experiment followed the guidelines of the Animal Care and Use Committee (ACUC) of Shanghai Minical Medical Research Co., Ltd. (approval number IACUC-MMIC-2023-94). Six Labrador canines with a mean weight of 25-35 kilograms, including five females. From one day before until three days after nsPEF ablation (nsPFA), the animals were administered analgesics, including carprofen (4 mg/kg orally), fentanyl (50 μg/h transdermally) and buprenorphine (0.01 mg/kg intramuscularly). Heparin was administered to maintain an activated clotting time between 250 and 350 seconds during the procedures. Subsequent to the administration of anesthesia, the animals were positioned in a supine position on the operating table and underwent endotracheal intubation, assisted ventilation, and Electrocardiography (ECG) recording (Abbott, Chicago, IL, USA).

2.2. Prototype of PIMSNA Devices

The study utilizes the PIMSNA device (RuiDi, Hangzhou, China), which comprises three components: a generator that delivers biphasic nsPEF energy via the ablation catheter's tip electrode, a connector that enables compatible focal ablation catheters and mapping systems to be connected, and a cardiac monitor that synchronizes nsPFA delivery with the R-wave (Figure 1A). The disposable

 doi:10.20944/preprints202511.2176.v1

electrical pulse ablation catheter is utilized for direct-contact ablation in the IVS, guided by real-time echocardiography. The electrode cable is connected to the nsPEF ablation instrument interface (Figure 1B).

2.3. Numerical Simulation of the nsPEF Distribution and the Potato Ablation

The COMSOL Multiphysics 6.1 (COMSOL, Sweden) was utilized to simulate the electric field of a single bipolar electrode needle in a vitro model, as described in an established scientific protocol [13]. The treatment entailed the application of a biphasic square-pulse electric field, characterized by a pulse width of 900 nanoseconds(ns) and a frequency of 1 Hertz(Hz). The electric field was configured to one of four levels: 2,000 volts/centimeter(V/cm), 3,000 V/cm, 4,000 V/cm, or 5,000 V/cm. The pulse interval was set to 5,000 ns and the number of pulses was set to between 100 and 300 to achieve a sufficient nsPEF ablated area. The determination was made through numerical simulation of the electric field distribution (Figure 1C).

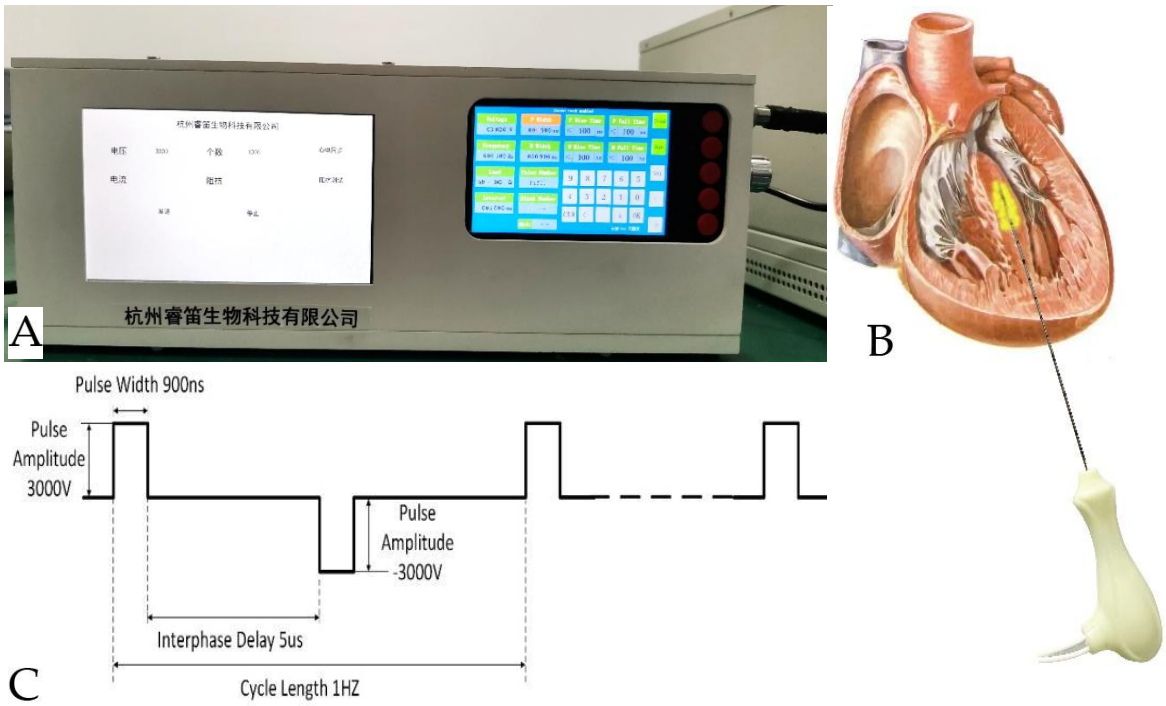

Figure 1. The Ruidi PIMSNA system. **(A)**.The generator weighs 10 kilograms. **(B)**. A 16G ablation electrode needle was utilized to deliver bipolar nsPEF ablation via alternating current. The electrode was inserted through the right ventricular apical region to the IVS. **(C)**. A sample pulse train was utilized for nsPEF ablation. A complete pulse consists of positive and negative pulses of equal amplitude and width that are separated by an interphase. Pulse release can occur at a constant frequency or at each ventricular refractory period. nsPEF, nanosecond pulsed electric field; PIMSNA, percutaneous intramyocardial septal nsPEF ablation; IVS, interventricular septum.

2.4. PIMSRA and PIMSRNA Procedure

2.4.1. PIMSRA Procedure

The canines were placed in the left lateral position, as previously described by the author [14]. The procedure involved the utilization of a 14-gauge, 14-centimeter-long Cool-tip RFA single electrode, equipped with a 0.7-centimeter impedance-controlled exposed tip, in conjunction with a radiofrequency generator (Cool-tip™ RF Ablation System; Medtronic Minimally Invasive Therapies, Minneapolis, MN, USA). Transthoracic echocardiography (TTE) (EPIQ7C; Philips, the Netherlands) with an S5-1 transducer (frequency: 5-1 MHz) was utilized to guide the procedure. Under the guidance of real-time echocardiography, a radiofrequency electrode needle was delicately inserted

 doi:10.20944/preprints202511.2176.v1

through the right ventricular apex of the chest wall and into the basal segment of the IVS. Subsequently, the RF electrode was inserted through the right ventricular apex to the basal segment of the IVS, guided by the puncture line. The ablation power ranged from 25 to 40 watts, with a maximum duration of five minutes per session. Each animal was subjected to a single ablation procedure. If ventricular arrhythmia occurred, the procedure was temporarily suspended and resumed upon its cessation. The canines received an intravenous saline infusion and any necessary medication to maintain hydration and prevent hypotension during the procedure.

2.4.2. PIMSNA Procedure

The PIMSNA procedure is similar to the PIMSRA technique [7]. The optimal route is defined as maintaining the long axis of the IVS in alignment with the puncture line as depicted in the echocardiography image. Pulse trains consist of a series of biphasic pulses, with a pulse width of 900 ns, an interphase delay of 5 μs, and a cycle length of 1 Hz. Each pulse train comprises of a positive 3,000 V pulse, followed by a negative 3,000 V pulse of reverse polarity. The total number of pulse trains delivered for each placement ranges from 100-300. The intensity of the ablation is determined by the number of pulses delivered. The efficacy of the ablation procedure is indicated by a 10% decline in electrode impedance.

2.5. End study

2.5.1. Impedance

Impedance alterations were meticulously monitored in real-time during the ablation procedures.

2.5.2. Arrhythmia monitor

ECG was performed during the procedure and follow-up to evaluate the presence of any arrhythmias.

2.5.3. Examination of TTE

Following the ablation procedure, contrast echocardiography (SonoVue, Bracco, Italy) was performed to assess the necrotic area by identifying myocardial perfusion defects in the ablated regions. TTE was performed before and after nsPFA, as well as seven days and three months afterwards, using an ultrasound system. The thickness, motion amplitude and systolic wall thickening rate of the ablated region were measured over three consecutive cardiac cycles.

2.5.4. Coronary angiography

Standard 6F guide catheters (Judkins left, Amplatz left or Extra Back-Up) were utilized for coronary angiography prior to and following the procedure. The left anterior oblique view was utilized to identify septal branch injuries [15]. At the 7-, 30-, and 90-day endpoints, the animals were anesthetized for coronary angiography.

2.5.5. Cardiac enzyme

Cardiac enzymes, including creatine kinase-MB isoenzyme (CK-MB) and α-hydroxybutyric acid (HBDH) dehydrogenase, were measured by a standard kit (Lumigenex Co., Ltd., Suzhou, China) both in PIMSRA and PIMSRNA before and after ablation. Blood samples (5 ml) were collected from the femoral vein prior to the ablation and at 3, 7, 14, and 30 days following the procedure.

2.6. Gross pathology and histopathology

Subsequent ablation procedure, each animal was closely monitored by a veterinarian. The animals exhibited no overt clinical signs until the scheduled euthanasia on days 7, 30, and 90 after the ablation procedure. This finding aligns with the results of our previous studies [16]. During the

 doi:10.20944/preprints202511.2176.v1

necropsy, cardiotomy was performed, and the ablated IVS tissue was subjected to gross and microscopic pathology evaluation. The width of the lesion was measured by cutting the tissue masses vertically in the direction of entry of the ablation electrodes. For microscopic observation, the IVS tissue was trimmed, and relevant sections were fixed in a 10% formalin solution for a minimum of three days. Subsequently, these sections were subjected to staining with hematoxylin and eosin, as well as Masson's trichrome, in order to evaluate pathological changes such as edema and thrombus under microscopic examination. The dimensions of the lesion were measured using CaseViewer 2.4 software (3DHISTECH, Hungary). The maximum depth perpendicular to the endocardium, measured in millimeters, was obtained from the digital images.

2.7. Statistical Analysis

The statistical analysis was conducted using SPSS version 20.0 (IBM Corporation, Armonk, NY, USA) software. The measurement data that conformed to a normal distribution was expressed as $\overline{x}$ ± SD, while the count data was described by frequency (composition ratio). Measurement data were compared between groups using a *t*-test, while count data were compared using the Chi-squared test or Fisher's test. The statistical significance was defined as $P < 0.05$.

3. Results

3.1. Numerical simulation and nsPFA of the potato

The electric field distributions were predicted by analogue simulation with an in vitro model, suggesting electric field strength 3,000 V and 5,000 V (Figure 2). The dose-effect on ablation area was measured (Figure 3A, 3B). When the voltage is beyond 5,000 V, firing and breakdown occurred (Figure 3C).

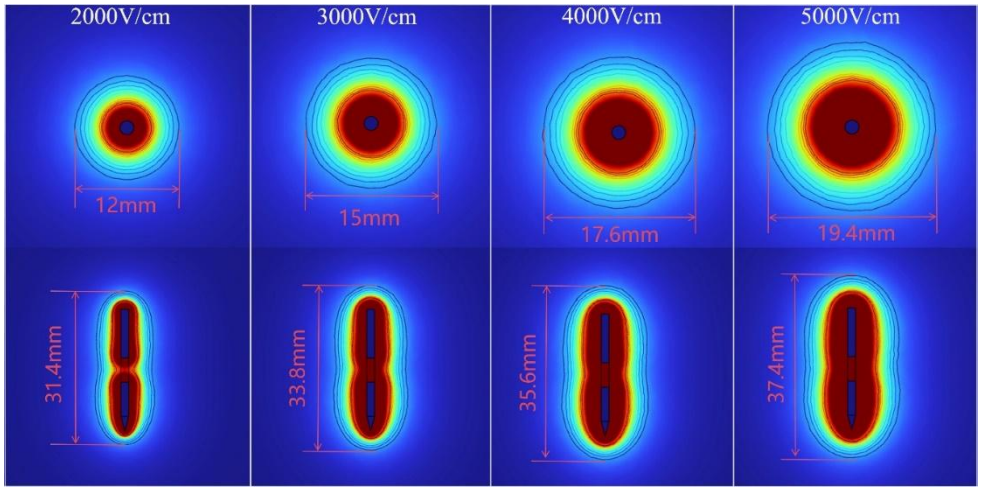

Figure 2. The simulation results demonstrate the distribution of nsPEF. A needle-like electrode is inserted into a potato. The maximum electric field is concentrated in the proximity of the electrode and increases with output voltage. nsPEF, nanosecond pulsed electric field.

 doi:10.20944/preprints202511.2176.v1

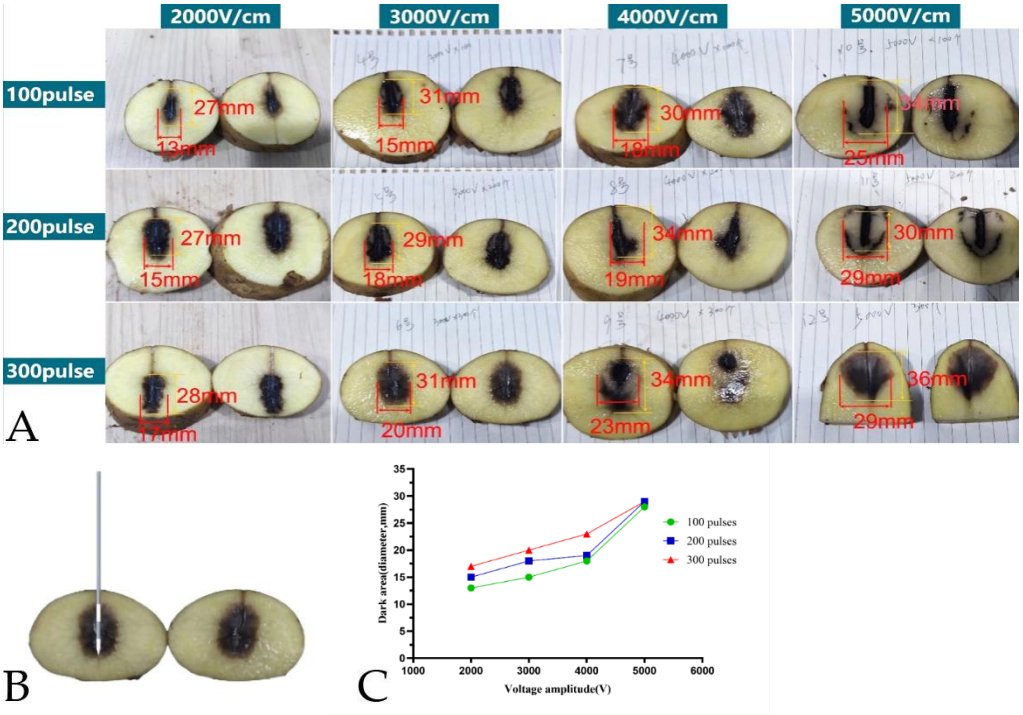

Figure 3. The relationship between nsPEF ablation strength and maximal damage diameter in potatoes. **(A)** The extent of the ablated area (melanin accumulation) in potato tissue was measured as a function of the number of pulses (100-300) and voltage (2,000 V, 5,000 V). **(B)** A schematic diagram illustrates the insertion of electrodes for potato ablation. **(C)** The provided diagram illustrates the ablation area and the percentage change in voltage amplitude. nsPEF, nanosecond pulsed electric field.

3.2. Ablation-Related Parameter Analysis

3.2.1. Impedance

During the process of ablation with nsPEF, the electrode's impedance undergoes a dynamic transformation. The impedance after nsPFA was lower than before nsPFA, and this difference was statistically significant (175.60 ± 24.52 Ω before nsPFA vs. 150.20 ± 21.90 Ω immediately after nsPFA, $P = 0.044$). Arrhythmia monitor: IVS ablation was performed directly using an ECG-gated approach. Premature ventricular contractions (PVCs) and ventricular tachycardia occurred on occasion during the procedure, with PVCs being the predominant manifestation. No instances of sustained ventricular tachycardia or ventricular fibrillation were observed during nsPFA or the survival period.

3.2.2. Echocardiographic Monitoring During Intra-Septal nsPFA

TTE examinations were performed throughout the procedure and at each subsequent follow-up (Figure 4A and 4B). Subsequent to the ablation procedure, the myocardial area exhibited increased echogenicity on the echocardiographic images that were generated. This change remained after 7 days. By contrast, no significant changes in echo intensity were observed in the non-ablated segments (Figure 4C and 4D). Postoperative contrast-enhanced echocardiography revealed no significant decrease in myocardial perfusion in the ablated area compared with the non-ablated region (Figure 4E and 4F). Furthermore, visual assessment of myocardial motion revealed a significant reduction in motion within the ablated region after the procedure, with septal hypokinesis observed after nsPFA. The thickness of the septum in the ablated region did not undergo significant change after nsPFA, immediately following the procedure (F = 1.506, $P = 0.375$, Figure 4G). The rate of systolic wall thickening and motion amplitude decreased significantly immediately following nsPFA, remaining at a lower level (systolic wall thickening rate: F = 15.283, $P = 0.000$; motion amplitude: The result of this calculation, F = 21.172, $P = 0.000$, is consistent with the findings presented in Fig 4H and4I).

 doi:10.20944/preprints202511.2176.v1

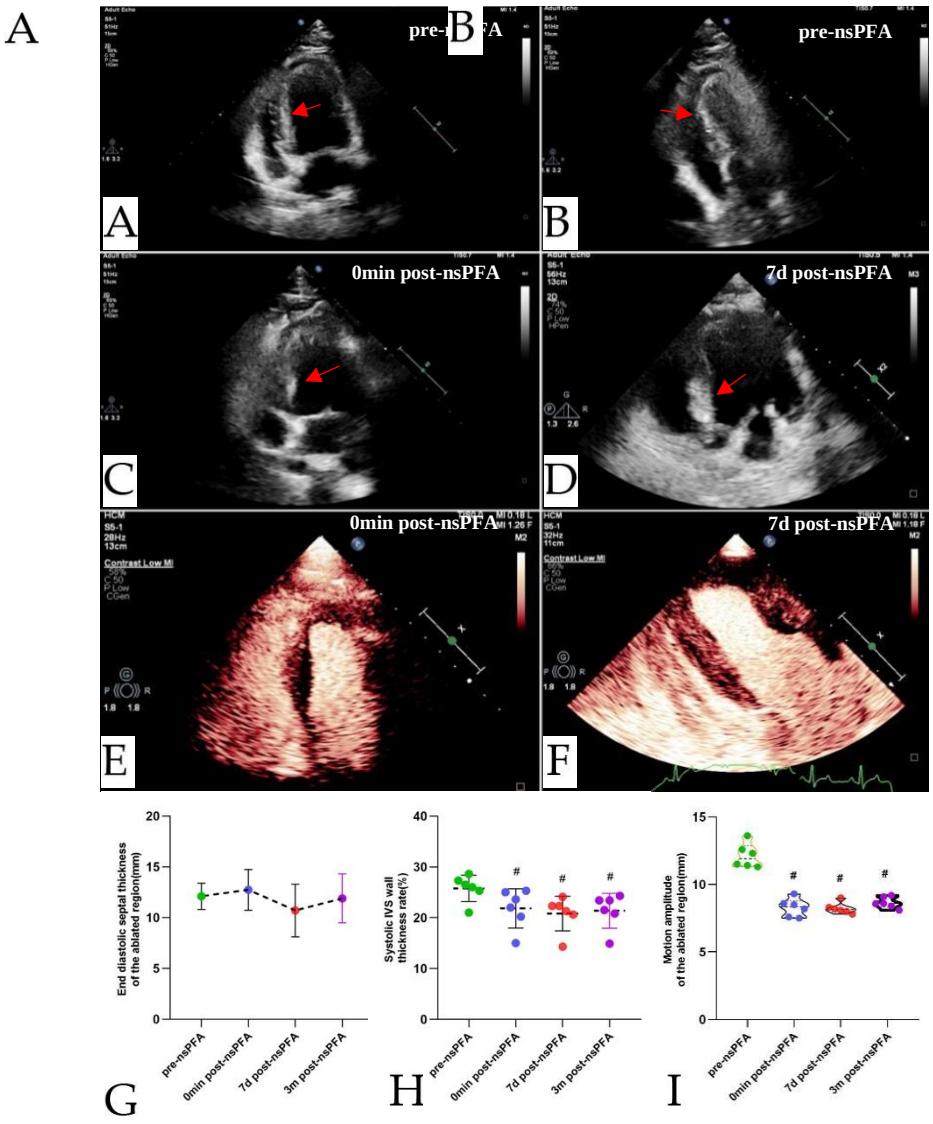

Figure 4. TTE-guided nsPEF ablation procedure. **(A).** During preoperative TTE, the apical four-chamber view revealed the left and right ventricles, as well as the IVS. **(B)**. The nsPFA electrode needle punctures the right ventricular apex of the chest wall and enters the basal segment of the IVS (red arrow). **(C)**. Immediately after ablation, the basal IVS exhibited a greater degree of brightness in comparison to the other myocardial segments, as evidenced by TTE image (red arrow). **(D)**. Enhanced echogenicity was still visible in the basal IVS seven days later with no significant changes in other segments (red arrow). Contrast-enhanced echocardiography showed no significant differences in myocardial perfusion between the basal IVS and other segments immediately **(E)** and seven days **(F)** following the ablation procedure. The septal thickness **(G)**, systolic wall thickness rate **(H)**, and motion amplitude **(I)** of the ablation region in the IVS are shown during nsPEF ablation. ($^{\#}P < 0.05$ vs. pre-nsPFA). nsPEF, nanosecond pulsed electric field; TTE, transthoracic echocardiography; IVS, interventricular septum.

3.2.3. Coronary Arteriography

Coronary arteriography revealed that septal branch vascularization was not significantly impacted neither RFA nor nsPFA (Figure 5).

 doi:10.20944/preprints202511.2176.v1

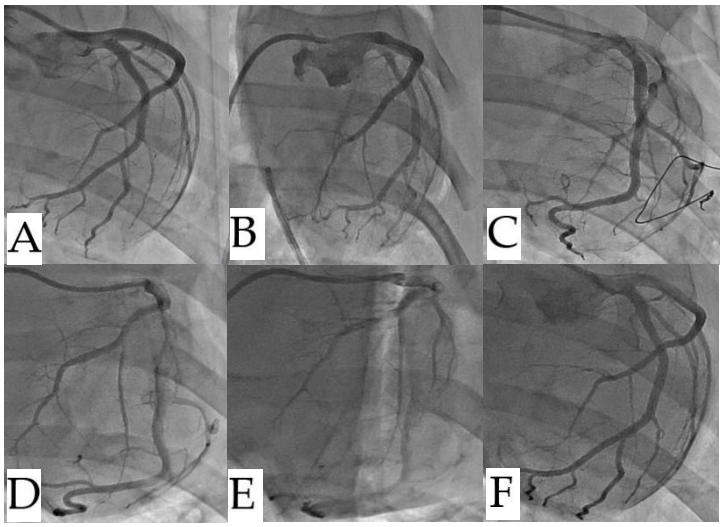

Figure 5. Comparison of coronary angiography before and after ablation. (Top row: RF ablation animal; Bottom row: nsPEF ablation animal). **(A,C).**before ablation, **(B,D).** immediately after ablation, and **(E,F).** seven days after ablation. There were no significant abnormalities found on left coronary septal branch angiography in either group. nsPEF, nanosecond pulsed electric field; RF, radiofrequency.

3.2.4. Cardiac Enzyme Profile Levels

Cardiac enzymes including CK-MB and HBDH, increased significantly in both the RFA and nsPFA groups at three days post-ablation, returning to preoperative levels at 14 days post-ablation. CK-MB levels were 13 times higher on 3 days post-ablation, decreased significantly thereafter and returned to preoperative levels at 14 days post-ablation. No statistically significant difference between the two groups in terms of CK-MB and HBDH ($P > 0.05$).

3.3. Gross Pathology and Pathological Findings

Histologically, the ablation procedure resulted in the complete absence of viable myocardial cells, which were replaced by homogeneous collagen adjacent to healthy myocardium within 3 to 90 days. On day 3 after ablation, clear boundaries lined up the nsPEF-ablated septal region and the surrounding myocardium (Figure 6A, 6C and 6D). Gross inspection revealed that the subendocardial ablations on the left ventricular surface of the IVS showed structural integrity (Figure 6B). No significant edema in the submucosa nor inflammation. The small arteries and veins appeared intact (Figure 6D, 6E and 6F). Seven days after ablation, the cardiac puncture site heal (Figure 7A). The subendocardial ablations of the right ventricular endocardial layer were preserved (Figure 7B), but the trans-endocardial ablation caused damage to the left ventricular endocardial surfaces. No adherent thrombus found (Figure 7C). After formalin fixation, the cross-section of the IVS specimen was examined. Masson trichrome staining was used to analyze the histology section. The results showed that the collagen fiber framework was fully retained and appeared contiguous across the septum, with sharp boundaries and little variation in width (Figure 7D). Histology confirmed transmural replacement fibrosis and revealed an abrupt transition to normal, untreated muscle (Figure 7E, F and 7G). Thirty days after the procedure, a clear boundary was evident between the nsPFA area and the surrounding myocardium (Figure 8A and 8C). The architecture of the intramural coronary arterioles and venules remained intact, with no evidence of luminal stenosis or occlusion within the myocardial ablation lesion (Figure 8B). Gradually, the ablation area was replaced with fibrous tissue from the edge, and the lesions could be clearly distinguished (Figure 8D). Ninety days after ablation, the ablated area had been completely replaced by homogenized fibrosis. The border between the ablated and normal myocardial tissue was clearly defined (Figure 9A, 9B). Blood flow was present in the arteries and veins within the ablated area. The specialized conduction tissue with

 doi:10.20944/preprints202511.2176.v1

preserved ultrastructure and intact nuclei is present within the myocardial ablation lesion (Figure 9C, 9D and 9E).

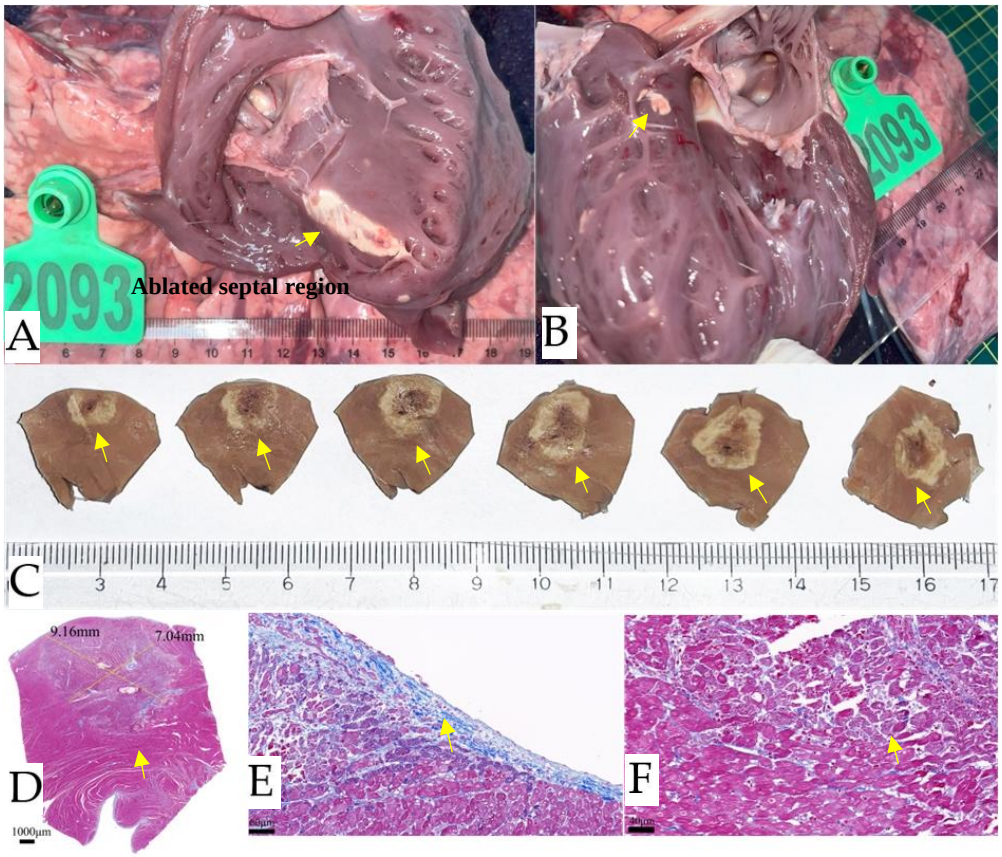

Figure 6. Tissue observed three days after intravascular non-thermal nsPEF ablation. Gross necropsy views show changes to the ventricular septum at sacrifice. **(A).** The gross appearance of nsPEF ablation lesions was observed after formalin fixation. **(B)**. Distinct sub-endocardial ablation lesions on the left ventricular surface of the IVS are visible on gross inspection, demonstrating structural integrity (yellow arrows). **(C)**. An obvious boundary can be seen between the nsPEF-ablated septal region and the surrounding myocardium. Masson's trichrome stain was used to examine nsPEF ablation sections. **(D)**.The ablation area measured 7.04×9.16 mm. **(E)**. Representative images show the normal and ablated myocardium, as well as the endocardial surface of the IVS after nsPEF ablation. **(F)**. The myocardium affected by nsPEF ablation maintained an approximately normal contour with gradually increased hyperchromatic cytoplasm and nuclear pyknosis. There is no significant edema in the submucosa, no any inflammatory cell infiltration. Small arteries and veins appear intact. nsPEF, nanosecond pulsed electric field; RF, radiofrequency; IVS, interventricular septum.

 doi:10.20944/preprints202511.2176.v1

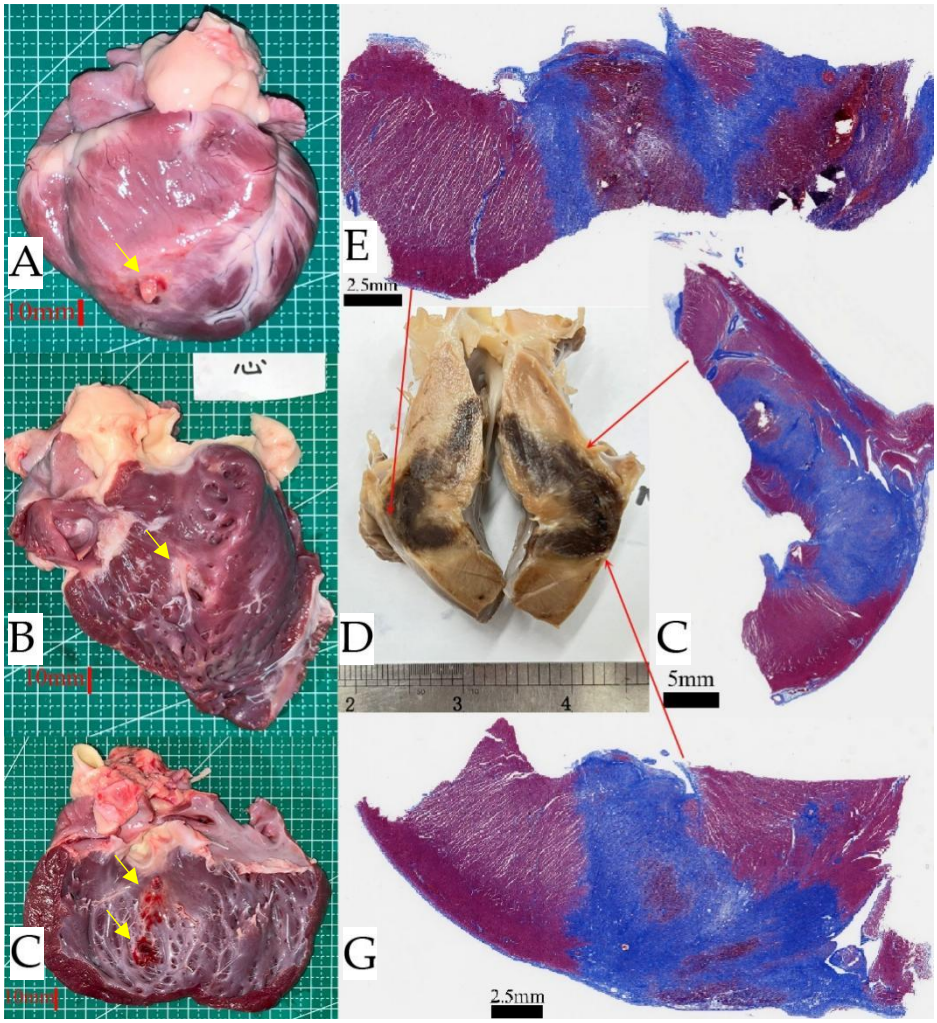

Figure 7. Tissue observation seven days after IVS non-thermal nsPEF ablation. (A). Gross pathology seven days after IVS ablation shows the cardiac puncture site in the process of repair, as indicated by the yellow arrows. **(B)**. Gross inspection reveals distinct lesions with structural integrity (yellow arrows) on the sub-endocardial ablations on the right ventricular surface of the IVS. **(C)**. Two distinct lesions (yellow arrows) are present on the left ventricular endocardial surface due to intracardiac trans-endocardial ablation of the IVS. **(D)**. Cross section of the IVS specimen after formalin fixation. The histology section clearly shows healthy myocardium (red) adjacent to myocardial ablation and a fully retained collagen fiber framework (blue) that appears contiguous across the septum. The boundaries are sharp, and the width varies little. Histology confirms transmural replacement fibrosis and shows an abrupt transition to normal, untreated muscle (**E, F, G**). IVS, interventricular septum; nsPEF, nanosecond pulsed electric field.

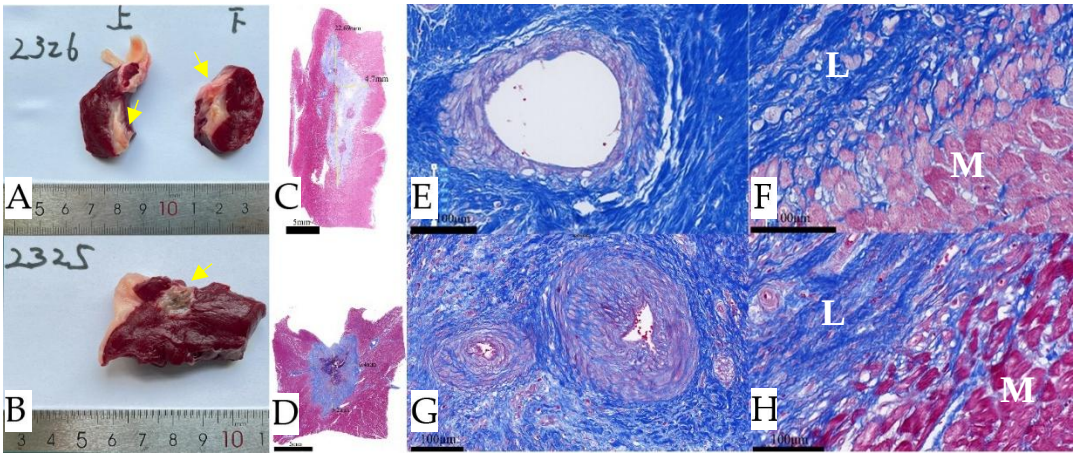

 doi:10.20944/preprints202511.2176.v1

Figure 8. Effect of nsPEF and RF ablation procedures on IVS at 30 days post-ablation. The top row shows the results of non-thermal nsPEF ablation, and the bottom row shows the results of RF ablation. In situ necropsy, **(A)**. A continuous ablation area is visible in the non-thermal nsPEF ablation, as indicated by the yellow arrow. **(B).** The thermal RF ablation lesion shows significant burns in the ablation center area. Masson's trichrome staining, **(C).**Homogeneous fibrosis is revealed after nsPEF ablation. **(D).** The RF lesion showed a predominantly fibrotic transmural lesion with islands of necrosis. Histology confirmed this after nsPEF ablation. **(E,F).** It confirmed replacement fibrosis and showed a clear ablation lesion (L) with an abrupt transition to normal, untreated healthy myocardium (M). The collateral damage profile was also observed. The photomicrograph of the artery showed no obvious pathological changes. **(G)**. RF ablation resulted in arterial wall remodeling, which was characterized by significant fibrosis and loss of media myocytes. **(H)**. The border region was not clearly defined. nsPEF, nanosecond pulsed electric field; RF, radiofrequency; IVS, interventricular septum.

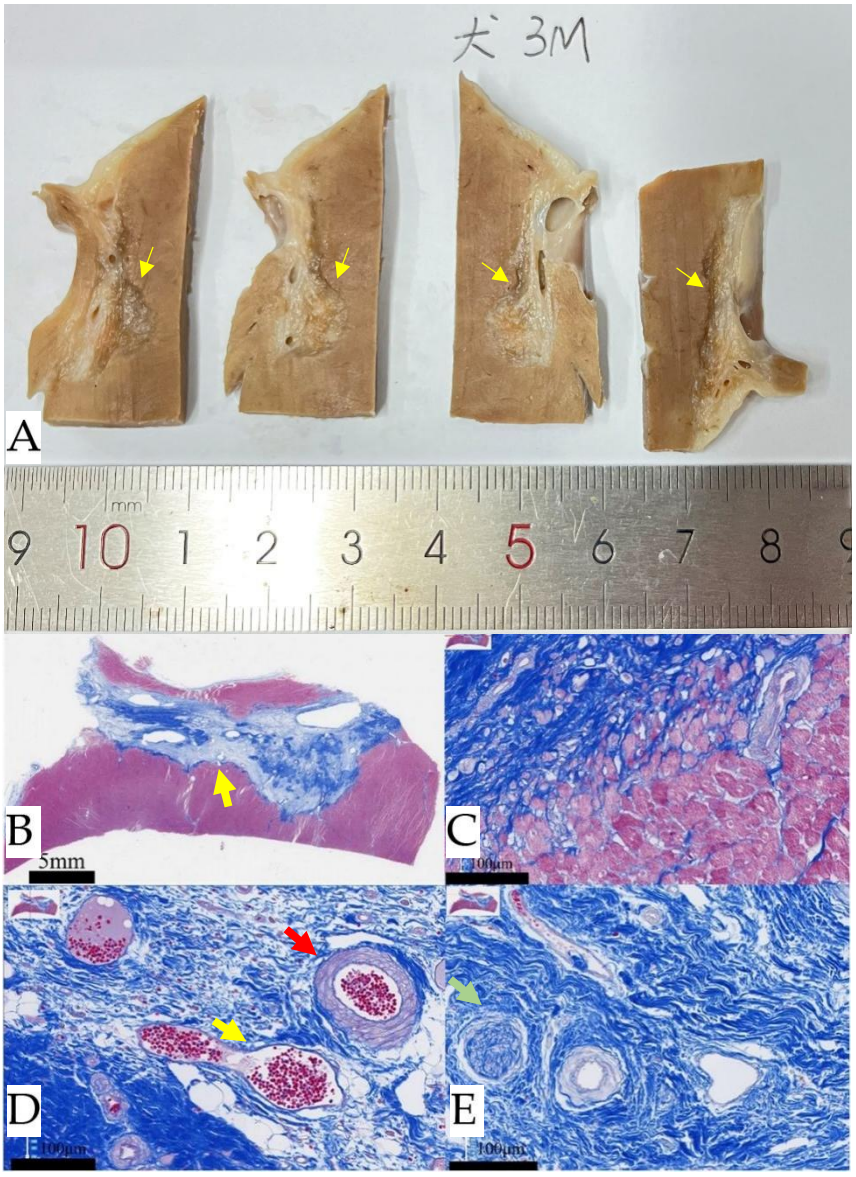

Figure 9. Gross pathology and histology of IVS 90 days after nsPFA. (A). A continuous ablation area is visible under the specimen after formalin fixation, as indicated by the yellow arrows. Masson's trichrome staining: **(B, C)**. Confirms replacement fibrosis and shows an abrupt transition to normal, untreated muscle. **(D, E).** In the region of ablation, the arterial (red arrows), venous (yellow arrows), and neural (green arrows) demonstrate notable resilience, maintaining the structural integrity. IVS, interventricular septum.

 doi:10.20944/preprints202511.2176.v1

4. Discussion

This pilot study demonstrates the feasibility of TTE-guided PIMSNA, a novel approach utilizing nanosecond pulsed electric field (nsPEF) ablation for SRT in HOCM to alleviate LVOT obstruction. The investigation thoroughly evaluated the ablation procedure, imaging characteristics, and histological features of TTE-guided PIMSNA within the interventricular septum. There was no occurrence of sustained ventricular tachycardia, ventricular fibrillation, or conduction block during nsPEF ablation or the subsequent survival period. nsPEF is safe and effective, when performed in the interventricular septum using a disposable catheter under TTE guidance.

The highlights of the investigation:

1. Preclinical animal studies definitively demonstrate that TTE-guided PIMSNA is safe, and efficacious.

2. We optimized the bipolar nsPEF ablation parameters to achieve an output of 3,000 V/cm.

3. A ≥10% reduction in impedance reliably indicates effective target tissue ablation.

4. Post-procedural TTE revealed no evidence of septal edema following PIMSNA.

5. Histological analysis confirmed the preservation of normal intramural coronary vasculature, viable neural tissue, and intact endocardial structures within nsPEF ablation lesions. No tissue edema was observed.

Here is the professionally polished text that adheres to all the specified requirements. PFA is a nonthermal ablation technique that selectively targets cardiomyocytes while preserving the extracellular matrix [17]. PFA affects all cellular constituents within a zone exposed to a sufficient electric field, achieving tissue selectivity based on tissue-specific electric field thresholds required for IRE [18]. The tissue specificity of PFA has been clinically validated in human atrial fibrillation ablation through experimental evidence. This technology presents potential for application in ventricular arrhythmia management [19].

A distinctive feature of nsPFA is that it exhibits the lowest electric field strength thresholds necessary to induce lethal electroporation among all tissue [10]. Cellular responses to nsPEF include calcium mobilization, cytoskeletal disruption, activation of signaling pathways, and induction of the apoptosis process, which may result in fibrosis. Cardiomyocytes exhibit lower electroporation thresholds than other tissues, thereby minimizing collateral damage to non-target structures, such as vascular and neural tissues. Ablation lesions generated by nsPFA demonstrate transmurality [9,20].

Three-dimensional (3D)-guided transvenous interseptal RFA and nonsurgical RFA utilizing solid-tip ablation catheters positioned bilaterally along the IVS can mitigate significant acute edema formation [11,12]. However, this approach entails a significant risk of atrioventricular conduction block. For symptomatic HOCM, TEE-guided PIMSRA constitutes an effective therapeutic intervention [21]. Nevertheless, PIMSRA carries risks including pulseless electrical activity cardiac arrest and pericardial tamponade. These risks are potentially attributable to ablation-induced tissue edema within the basal IVS and hemorrhagic complications arising from puncture-related vascular injury [22]. Furthermore, the development of an IVS hematoma necessitates immediate clinical intervention [23].

The authors developed a novel technique designated PIMSNA. The ablation methodology paralleled PIMSRA [7]. A 16-gauge nsPFA electrode needle (Ruidi PEF Ablation System) was introduced percutaneously via a transapical intramyocardial approach. nsPEF energy delivery was restricted to the needle tip. TTE guidance was used throughout the procedure to prevent vascular injury and atrioventricular conduction impairment at the needle insertion site. This study introduces the PIMSNA technique for reducing ventricular septal masses. Preclinical findings demonstrate that this procedure effectively and safely induces targeted septal cardiomyocyte death without eliciting acute thickening in the ablated region. Histological analysis confirmed that nsPFA did not produce significant myocardial edema and was associated with a minimal inflammatory response. Additionally, our prior investigations revealed a consistent pattern of programmed cardiomyocyte death, wherein cardiomyocytes predominantly underwent apoptosis, followed by secondary necrosis [16]. The ablation zone exhibited a sharply demarcated boundary, and the lesioned area was

 doi:10.20944/preprints202511.2176.v1

subsequently replaced by structurally intact fibroblastic tissue. Notably, vascular and neural structures within the ablation field remained unaffected.

In this study, we performed non-surgical nsPFA directly within the IVS using ECG-gating. We observed PVCs and non-sustained ventricular tachycardia during ablation, with PVCs being the main manifestation. There were no instances of sustained ventricular tachycardia or ventricular fibrillation.

The PIMSNA procedure boasts several key advantages. It uses three-dimensional echocardiography to precisely delineate the nsPFA target region. This enhances ablation accuracy and mitigates potential injury to the conduction system. Furthermore, performing the ablation manipulation within the IVS facilitates procedural simplification and reduces the risk of thromboembolic complications, such as stroke.

4.1. Limitations

This study has several limitations that warrant consideration. First, the procedure was evaluated only in the non-obstructive septum of healthy canine subjects. Monitoring the LVOT pressure gradient was not possible due to the lack of a suitable large animal model of HOCM. It is important to emphasize that these limitations do not diminish the significance of the study's core findings. The effective myocardial injury achieved in the septal myocardium in this study nonetheless provides a foundation for SRT. Second, the prototype catheter design was based on normal septal thickness parameters. In scenarios involving hypertrophic ventricular septum, increasing the inter-electrode distance may be necessary to expand the effective PFA lesion area. Significant interspecies variation in response to nsPFA must be acknowledged. Consequently, the ablation parameters employed in this study, especially the redesigned inter-electrode spacing, cannot be directly extrapolated to humans. Nevertheless, our findings collectively suggest that this novel procedure is a feasible and safe approach to SRT.

5. Conclusions

This study introduces a novel technique for percutaneous, nonthermal, intramyocardial septal nsPFA and demonstrates its efficacy, safety and feasibility. Using 3D transthoracic echocardiography for guidance, the procedure selectively injures the myocardium and induces localized hypokinesis without evident edema. The ablation zone attenuates fibrotic progression while preserving vascular integrity. nsPFA-mediated cardiomyocyte death exhibits a characteristic apoptotic pattern accompanied by negligible inflammatory infiltration.

Author Contributions: All authors discussed in advance the topics to be discussed and how best to address them. Conceptualization and study design, Z.Z., X.C. and Z.P.; data collection, X.X., G.Q., J.L., S.L., X.L., B.W.; data analysis, Z.Z., Z.P., X.C. and Y.C.; manuscript—preparation, Z.Z., X.X. and Z.P. The manuscript was approved by all the above authors. All authors have read and agreed to the published version of the manuscript.

Funding: This work was supported by the National Key R&D Program of China, Grant/Award(No. 8247022200), Zhejiang Medical Association Clinical Medical Research Funds (No. 2024ZYC-Z14), Hangzhou Medicine and Health Science and Technology Funds (No. ZD20250246).

Institutional Review Board Statement: The animal study protocol was approved by the Animal Care and Use Committee (ACUC) of Shanghai **Mincal Medical** Research Co., Ltd. Large Animal Research Center[Approval IACUC-MMIC-2023-94]. The study adhered to the guidelines set by the committee.

Informed Consent Statement: Not applicable.

Data Availability Statement: The raw data supporting the conclusions of this article will be made available by the authors without undue reservation.

 doi:10.20944/preprints202511.2176.v1

Acknowledgments: We thank Liangjie Hong for coordinating the experiments and supervising and maintaining the animal laboratory. Thanks to Hangzhou Ruidi Biotechnology Co., Ltd. provided all PIMSNA devices throughout the study period.

Conflicts of Interest: The authors declare no conflict of interest.

Abbreviations

The following abbreviations are used in this manuscript:

HOCM	Hypertrophic obstructive cardiomyopathy
IRE	irreversible electroporation
PEF	Pulsed Electric Fields
nsPEF	Nanosecond pulsed electric field
nsPFA	nsPEF ablation
PIMSNA	percutaneous intramyocardial septal nsPEF ablation
PIMSRA	Percutaneous intramyocardial septal radiofrequency ablation
RFA	radiofrequency ablation
LVOT	left ventricular outflow tract
SRT	septal reduction therapy
IVS	interventricular septum
ECG	

References

1. Zhang, Y.;Zhang, X.;Zhao, Z. Emerging technologies for septal reduction therapy in hypertrophic cardiomyopathy. *Chin Med J (Engl)* **2025**, 138:2511-3.
2. Ommen, S.R.;Ho, C.Y.;Asif, I.M.;Balaji, S.;Burke, M.A.;Day, S.M.;Dearani, J.A.;Epps, K.C.;Evanovich, L.;Ferrari, V.A. et al. 2024 AHA/ACC/AMSSM/HRS/PACES/SCMR Guideline for the Management of Hypertrophic Cardiomyopathy: A Report of the American Heart Association/American College of Cardiology Joint Committee on Clinical Practice Guidelines. *J Am Coll Cardiol* **2024**, 83:2324-2405.
3. Bleszynski, P.A.;Goldenberg, I.;Fernandez, G.;Howell, E.;Younis, A.;Chen, A.Y.;McNitt, S.;Bruckel, J.;Ling, F.;Cove, C. et al. Risk of arrhythmic events after alcohol septal ablation for hypertrophic cardiomyopathy using continuous implantable cardiac monitoring. *Heart Rhythm* **2021**, 18:50-56.
4. Chen, J. Alcohol septal ablation for obstructive hypertrophic cardiomyopathy: Outdated technique or promising future? *Int J Cardiol* **2025**, 434:133358.
5. Yang, H.;Yang, Y.;Xue, Y.;Luo, S. Efficacy and safety of radiofrequency ablation for hypertrophic obstructive cardiomyopathy: A systematic review and meta-analysis. *Clin Cardiol* **2020**, 43:450-458.
6. Fang, J.;Liu, Y.;Zhu, Y.;Li, R.;Wang, R.;Wang, D.W.;Song, Y.;Li, C.;Chen, Y.;Cheng, L. et al. First-in-Human Transapical Beating-Heart Septal Myectomy in Patients With Hypertrophic Obstructive Cardiomyopathy. *J Am Coll Cardiol* **2023**, 82:575-586.
7. Zhou, M.;Ta, S.;Hahn, R.T.;Hsi, D.H.;Leon, M.B.;Hu, R.;Zhang, J.;Zuo, L.;Li, J.;Wang, J. et al. Percutaneous Intramyocardial Septal Radiofrequency Ablation in Patients With Drug-Refractory Hypertrophic Obstructive Cardiomyopathy. *JAMA Cardiol* **2022**, 7:529-538.
8. Wittkampf, F.H.M.;van Es, R.;Neven, K. Electroporation and its Relevance for Cardiac Catheter Ablation. *JACC Clin Electrophysiol* **2018**, 4:977-986.
9. Varghese, F.;Philpott, J.M.;Neuber, J.U.;Hargrave, B.;Zemlin, C.W. Surgical Ablation of Cardiac Tissue with Nanosecond Pulsed Electric Fields in Swine. *Cardiovasc Eng Technol* **2023**, 14:52-59.

 doi:10.20944/preprints202511.2176.v1

10. Xu, M.;Xu, D.;Dong, G.;Ren, Z.;Zhang, W.;Aji, T.;Zhao, Q.;Chen, X.;Jiang, T. The Safety and Efficacy of Nanosecond Pulsed Electric Field in Patients With Hepatocellular Carcinoma: A Prospective Phase 1 Clinical Study Protocol. *Front Oncol* **2022**, 12:869316.
11. Chang, R.;Luo, D.;He, W.;Tang, W.;Chen, J.;Li, J.;Liu, M.;Zhang, X.;Chen, X.;Su, C. et al. A novel method for septal reduction therapy by three-dimensional guided transvenous intraseptal pulsed-field ablation. *Heart Rhythm* **2024**, 21:258-267.
12. van Zyl, M.;Ladas, T.P.;Tri, J.A.;Yasin, O.Z.;Ladejobi, A.O.;Tan, N.Y.;Christopoulos, G.;Schneider, N.;Danitz, D.J.;Uecker, D. et al. Bipolar Electroporation Across the Interventricular Septum: Electrophysiological, Imaging, and Histopathological Characteristics. *JACC Clin Electrophysiol* **2022**, 8:1106-1118.
13. Lv, Y.;Yao, C.;Rubinsky, B. A Conceivable Mechanism Responsible for the Synergy of High and Low Voltage Irreversible Electroporation Pulses. *Ann Biomed Eng* **2019**, 47:1552-1563.
14. Xu, Y.;Yu, T.Y.;Pu, Z.X. Percutaneous Intramyocardial Septal Radiofrequency Ablation Relieving Residual Left Ventricular Outflow Tract Obstruction Following Alcohol Septal Ablation. *CASE (Phila)* **2022**, 6:340-343.
15. Arevalos, V.;Rodriguez-Arias, J.J.;Brugaletta, S.;Micari, A.;Costa, F.;Freixa, X.;Masotti, M.;Sabate, M.;Regueiro, A. Alcohol Septal Ablation: An Option on the Rise in Hypertrophic Obstructive Cardiomyopathy. *J Clin Med* **2021**, 10:2276.
16. Zhao, Z.;Chen, Y.;Wu, B.;Qiu, G.;Hong, L.;Chen, X.;Zhang, X. Pulsed-Field Ablation Using a Novel Ablation-Mapping Integrated System for Pulmonary Vein Isolation-A Preliminary Animal Study. *J Cardiovasc Dev Dis* **2022**, 9:425.
17. Buch, E.;Tandri, H. The Promise of Pulsed Field Ablation: Optimizing the Balance Between Efficacy and Safety. *JACC Clin Electrophysiol* **2023**, 9:649-651.
18. Ramirez, F.D.;Reddy, V.Y.;Viswanathan, R.;Hocini, M.;Jais, P. Emerging Technologies for Pulmonary Vein Isolation. *Circ Res* **2020**, 127:170-183.
19. Kautzner, J.;Peichl, P. Pulsed Field Ablation in Ventricular Arrhythmias. *Card Electrophysiol Clin* **2025**, 17:205-212.
20. Xie, F.;Varghese, F.;Pakhomov, A.G.;Semenov, I.;Xiao, S.;Philpott, J.;Zemlin, C. Ablation of Myocardial Tissue With Nanosecond Pulsed Electric Fields. *PloS one* **2015**, 10:e0144833.
21. Li, J.;Zhang, J.;Shi, Y.;Sievert, H.;Taub, C.C.;Bertog, S.;Ta, S.;Changhui, L.;Senser, E.;Wang, J. et al. Myocardial mechanics of percutaneous intramyocardial septal radiofrequency ablation. *Heart* **2023**, 109:289-296.
22. Shu, T.;Shen, C.;Chen, X.;Yu, F. Two severe complications post-percutaneous intramyocardial septal radiofrequency ablation in a patient with failed alcohol septal ablation: pulseless electrical activity cardiac arrest and pericardial tamponade-a case report. *Eur Heart J Case Rep* **2023**, 7:ytad371.
23. Wu, B.;Zhou, Y.;Lu, J.;Cui, Y.;Zhou, Z.;Lin, W.;Ma, L.;Xie, X.;Guo, X. Interventricular Septal Hematoma Caused by Percutaneous Intramyocardial Septal Radiofrequency Ablation Successfully Treated With Coil Embolization. *JACC Cardiovasc Interv* **2023**, 16:722-724.